Available online at www.sciencedirect.com
ScienceDirect
Journal of the European Ceramic Society 29 (2009) 3091–3097
www.elsevier.com/locate/jeurceramsoc

# Microstructure and mechanical properties of C/C–SiC composites fabricated by a rapid processing method

Jiping Wang [a,b,*], Min Lin [a], Zhuo Xu [b], Yonghui Zhang [a], Zhongqi Shi [a], Junmin Qian [a], Guanjun Qiao [a], Zhihao Jin [a]

[a] *State Key Laboratory for Mechanical Behavior of Materials, Xi'an Jiaotong University, Xi'an 710049, China*
[b] *Electronic Materials Research Laboratory, School of Electronics and Information Engineering, Xi'an Jiaotong University, Xi'an 710049, China*

Received 9 September 2008; received in revised form 21 April 2009; accepted 28 April 2009
Available online 26 May 2009

**Abstract**

C/C–SiC composite was fabricated with time efficiency and low cost by a two-step process. A quasi 3D carbon-fiber-felt was firstly densified to C/C composite in 2–5 h by a thermal gradient CVI method based on precursor of kerosene. Then, the C/C composite of different porosities was reactively infiltrated with Si for 40 min to obtain C/C–SiC composite. The influence of the porosity of the C/C composite on the microstructure and mechanical properties of the C/C–SiC composite was investigated. The results show that the density of the C/C–SiC composite increases from 2.0 g/cm$^3$ to 2.3 g/cm$^3$ while its porosity decreases from 5.8% to 1.7% with the increasing porosity of the C/C composite. Moreover, the porosity of the C/C composite affects both the amounts of β-SiC, Si phases and the mechanical properties of the C/C–SiC composite. The flexural strength and modulus of the C/C–SiC composite are much higher than those of the C/C composite. The C/C–SiC composite from the C/C composite of 19.7% porosity has the highest flexural strength and modulus, which are 132 MPa and 14.4 GPa, respectively.


*Keywords:* Carbon–carbon; SiC; Chemical vapor infiltration; Microstructure; Mechanical property

## 1. Introduction

C/C–SiC composites are widely used as structural materials in aerospace area for their outstanding properties,[1] such as high strength at elevated temperature, low density and superior toughness. C/C–SiC composites are also promising candidates for advanced brake and clutch systems.[2–4] Compared with C/C composites, C/C–SiC composites show more stable friction coefficient because their low open porosity restricts the ingress of oxygen and humidity which are harmful to their stability.[1,5]

Usually, the fabrication procedure of C/C–SiC composite includes two steps: preparing porous C/C composite and subsequent C/C–SiC composite. Chemical vapor infiltration (CVI) technique[6] is a primary route for preparing C/C composite. However, this method is costly because long period and several cycles are necessary to obtain sufficiently high density of C/C composite. Therefore, much efforts have been made to reduce manufacturing cost in order to expand the application areas of C/C composite.[6,7] On the other hand, to fabricate C/C–SiC composite[8–11] from porous C/C composite, reactive melt infiltration (RMI), or called liquid silicon infiltration (LSI) process,[12–14] is an attractive method considering the processing time and the cost. It is a near-net shaping process and one infiltration cycle can achieve fully dense products. In this method, porous C/C composite is impregnated with molten silicon, and C and Si reacts to form SiC at high temperature (above 1410 °C). The kinetics of liquid Si infiltration into porous carbon and the reaction mechanism between solid carbon and liquid Si have been extensively investigated.[15–18]

Recently, we presented a new method to carry out a rapid densification process of C/C composite by a thermal gradient CVI method based on precursor of vaporized kerosene.[19,20] By this method, the density of C/C composite can be increased to 1.71 g/cm$^3$ in 6 h.[19,20] Combining this new CVI process with RMI method, we have prepared C/C–SiC composite in several hours.[21,22] Therefore, the processing period and cost of C/C–SiC

* Corresponding author at: State Key Laboratory for Mechanical Behavior of Materials, Xi'an Jiaotong University, Xi'an 710049, China.
Tel.: +86 29 82668614; fax: +86 29 82663453.
*E-mail address:* jipingwang@gmail.com (J. Wang).

0955-2219/$ – see front matter © 2009 Elsevier Ltd. All rights reserved.
doi:10.1016/j.jeurceramsoc.2009.04.036

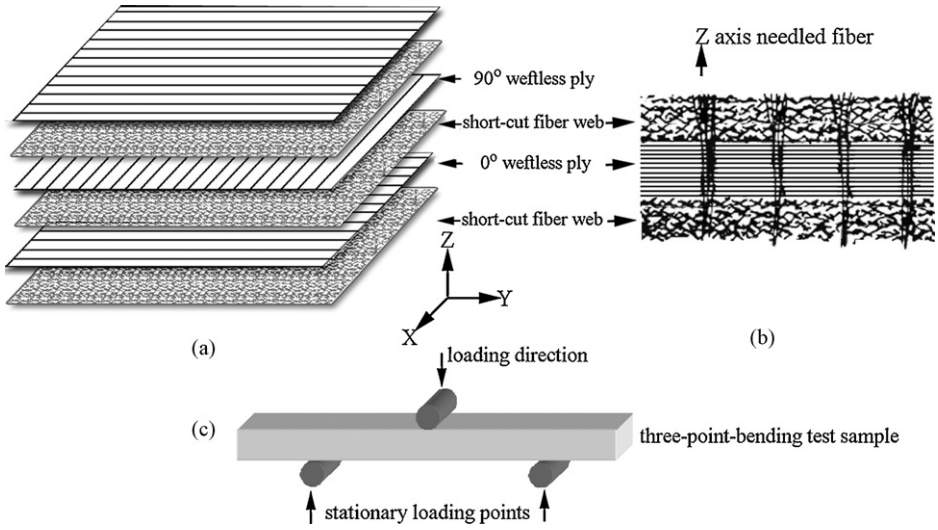


Fig. 1. Schematic diagram of the needle-punched quasi 3D carbon-fiber-felt. (a) The position of weftless ply and short-cut fiber web; (b) needle-punched carbon fiber of *Z*-axis integrated the different layers in a cross-section of *Y–Z* plane; (c) the relative position between the loading direction and C/C composite or C/C–SiC composite during three-point-bending test.

composite can be reduced sharply. However, the effects of the processing parameters on the contents and distribution of different phases (SiC, Si and pyrocarbon) in matrix and the mechanical property of the resulting C/C–SiC composite have not been well investigated.

In the present work, C/C composites with different porosities were made firstly by our CVI method in 2–5 h. C/C–SiC composites were prepared from the C/C composite by RMI processing. The influence of the porosity of C/C composite on the microstructure and mechanical properties of the C/C–SiC composite were systematically studied. As a result, we can obtain an optimized porosity of C/C composite for preparing C/C–SiC composite with excellent properties.

## 2. Experimental procedure

### 2.1. Material preparation

A needle-punched quasi 3D carbon-fiber-felt was chosen as reinforcement. The felt was made by repeatedly overlapping the layers of 0° weftless ply, short-cut fiber web and 90° weftless ply in *X–Y* plane with needle-punching on *Z*-axis direction step by step to a certain thickness. The schematic diagram of the felt is shown in Fig. 1(a) and (b). The fiber type was PAN-based carbon fiber whose diameter was ~7 μm, and fiber volume fraction in the felt was about 30%.

The C/C–SiC composite was fabricated by a two-step procedure, and the processing route is shown in Fig. 2.

*Step 1*: The felt (size: Ø100 mm × 10 mm) was densified into C/C composite by a thermal gradient CVI method with vaporized kerosene as a precursor. The detail of the method was described in our earlier literature.[20] The deposition temperature was ~1100 °C and the infiltration time was 2 h, 3 h, 4 h and 5 h.

*Step 2*: The C/C composite in size of 6 mm × 6 mm × 50 mm was placed in a graphite crucible and covered with some Si powder with a diameter range of 0.5–2 mm. Then the crucible was heated to 1550 °C in a furnace and held at this temperature for 40 min under vacuum atmosphere. After the Si RMI processing, C/C–SiC composites were prepared and named as CS-2, CS-3, CS-4, and CS-5 according to the C/C composite whose CVI time was 2 h, 3 h, 4 h, and 5 h, respectively.

### 2.2. Characterization

The density and open porosity of the C/C composite and the C/C–SiC composite were measured by Archimedes method

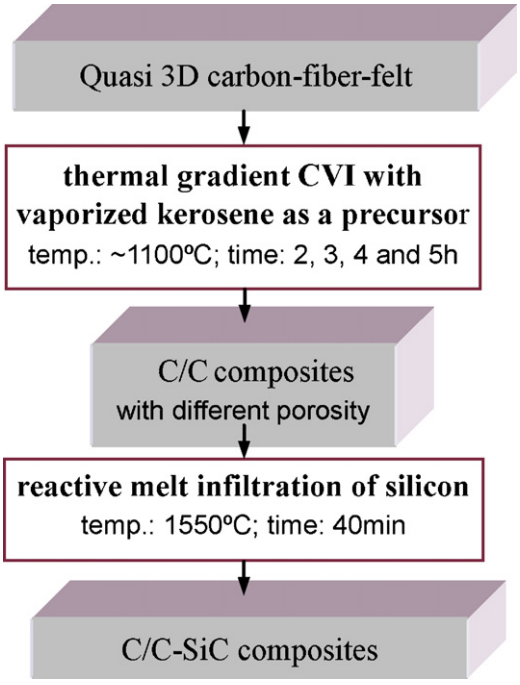


Fig. 2. Processing scheme of manufacturing C/C–SiC composites.

using distilled water. The C/C–SiC composite was examined via X-ray powder diffraction (XRD, D/MAX-RA X-ray diffractometer) between 15° and 70° (2$\theta$) using Cu $K_\alpha$ radiation.

The flexural strength and modulus of the C/C composite and C/C–SiC composite were measured by three-point-bending test at room temperature on an electron universal testing machine (Instron 1195). The dimension of the test sample was 5 mm ($B$) × 4 mm ($H$) × 50 mm. The span $L$ is 30 mm, and the crosshead speed is 0.5 mm/min. The relative position between the loading direction and C/C composite and C/C–SiC composite test samples is illustrated in Fig. 1(c). Flexural strength ($\sigma_f$) and flexural modulus ($E_f$) are calculated with the following equations:

$$\sigma_f = \frac{3PL}{2BH^2} \quad (1)$$

$$E_f = \frac{\Delta PL^3}{4BH^3\Delta f} \quad (2)$$

where $P$ is the maximum load, $\Delta P/\Delta f$ is the slope of the straight line in the load–deflection curve recorded during the test. All the flexural strength and modulus are the average values from five sample tests. The error-bars indicate the standard deviation.

After three-point-bending test, the polished surface parallel to $X$–$Z$ plane (see Fig. 1(c)) of the C/C–SiC sample was observed by an optical microscope (OM, Reichert, MeF3). The fracture surface of the C/C–SiC composite was observed by means of a scanning electron microscope (SEM, Hitachi, S-2700) operated at 25 kV and 20 mA.

## 3. Results and discussion

### 3.1. Open porosity and pyrocarbon volume ratio of C/C composite

Table 1 gives densities and the open porosities of the C/C composites prepared by the CVI processing. It shows that as the CVI time increases from 2 h to 5 h, the density of the C/C composite increases from 1.04 g/cm$^3$ to 1.65 g/cm$^3$, while its open porosity decreases from 37.6% to 15.3%. The deposition rate is much higher than that of normal CVI method.[20] The pyrocarbon (PyC) volume ratios ($V_{PyC}$) in the C/C composites are also shown in Table 1. $V_{PyC}$ is calculated by the following equation:

$$V_{PyC} = \frac{D_{C/C} - D_{Felt}}{D_{PyC}} \times 100\ \% \quad (3)$$

where $D_{C/C}$, $D_{Felt}$ and $D_{PyC}$ are the densities of C/C composite, carbon felt and PyC, respectively. $D_{Felt}$ is 0.51 g/cm$^3$, depending on the used carbon fiber and fiber volume ration. The PyC is rough laminar carbon structure, and its density ($D_{PyC}$) is 2.10 g/cm$^3$.[6,19,20] It can be seen from the table that with the increase of CVI time, $V_{PyC}$ value increases, leading to a higher density and a lower open porosity of the C/C composite.

Table 1
Densities, porosities and $V_{PyC}$ values of C/C composites.

| CVI time (h) | Density (g/cm$^3$) | Open porosity (%) | $V_{PyC}$ (%) |
|---|---|---|---|
| 2 | 1.04 | 37.6 | 25.2 |
| 3 | 1.31 | 29.4 | 38.1 |
| 4 | 1.54 | 19.7 | 49.0 |
| 5 | 1.65 | 15.3 | 54.3 |

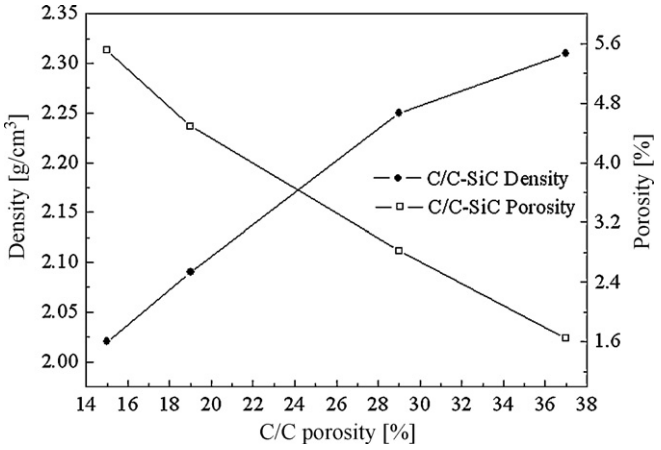


Fig. 3. Densities and open porosities of C/C–SiC composites vs. open porosities of C/C composites.

### 3.2. Density and Si volume ratio of C/C–SiC composite

The relationships between the densities and open porosities of the C/C–SiC composites and the open porosities of the C/C composites are shown in Fig. 3. With the increase of porosity of the C/C composite, the density of the C/C–SiC composite increases from 2.02 g/cm$^3$ to 2.31 g/cm$^3$, and is much higher than that of the C/C composite. The increment in density was directly attributed to the infiltration of Si. During the RMI processing, molten Si infiltrated into porous C/C composite via capillarity and simultaneously reacted with C to form SiC. The related Si volume ratio ($V_{Si}$) in the C/C–SiC composite can be calculated by the following equation

$$V_{Si} = \frac{D_{C/C\text{–}SiC} - D_{C/C}}{D_{Si}} \times 100\ \% \quad (4)$$

where $D_{Si}$ = 2.33 g/cm$^3$ is the density of cubic Si at room temperature, $D_{C/C\text{–}SiC}$ and $D_{C/C}$ are the densities of the C/C–SiC composite and the C/C composite, respectively. The $V_{Si}$ values are shown in Fig. 4. It reveals that C/C composite of high porosity can be infiltrated with more Si, which results in a higher density of C/C–SiC composite.

Fig. 3 also shows that the open porosities of the C/C–SiC composites are in the range of 5.5–1.6%, which decreases when the porosity of the C/C composite increases. SiC layer was formed on the surface of solid carbon during the RMI processing.[21,22] Its volume is two times larger than that of the carbon.[13] Therefore, the pore diameter in C/C composite was reduced and the Si infiltration became difficult or even stopped as the average pore diameter in the C/C composite became smaller. Unavoidably, some open pores remain in the C/C–SiC composite after RMI processing. Furthermore, Si infiltration is more difficult for the C/C composite of the lowest porosity (15.3%), resulting in

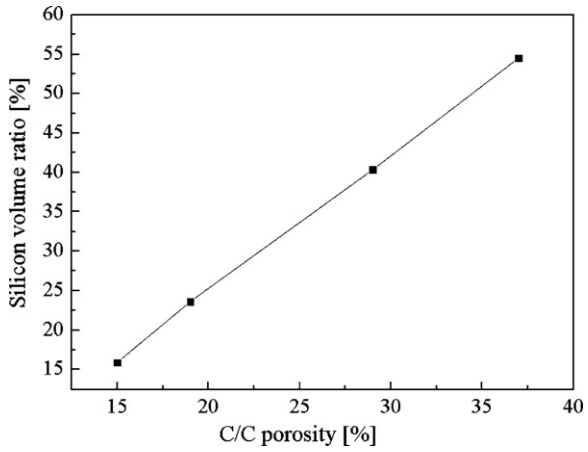


Fig. 4. $V_{Si}$ values of C/C–SiC composites vs. open porosities of C/C composites.

the highest open porosity of C/C–SiC composite (CS-5 sample) among the four types of composites.

### 3.3. XRD analysis of C/C–SiC composite

The XRD patterns of the C/C–SiC composites are shown in Fig. 5. It reveals that β-SiC phase was formed and unreacted Si phase and C (graphite) phase remained in the C/C–SiC composite. Comparing the patterns from CS-2 to CS-5 sample, one can see that the intensity of (0 0 2) peak of C phase increases while the intensity of (1 1 1) peak of Si phase decreases. It indicates that the relative content of C, Si and SiC in the C/C–SiC changed with the porosity of the C/C composite. CS-2 sample infiltrated the most of amount of Si among four types of the composites

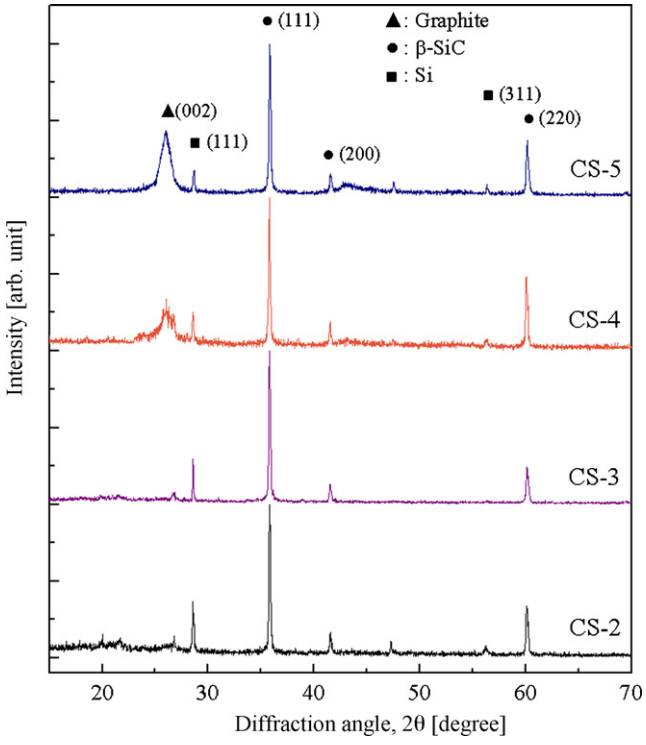


Fig. 5. XRD patterns of C/C–SiC composites.

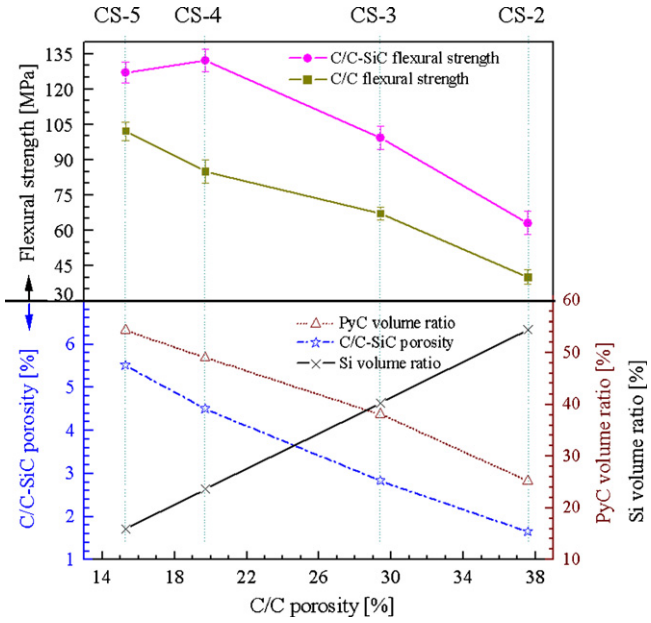


Fig. 6. Flexural strengths of C/C composites and C/C–SiC composites, $V_{Si}$ values, $V_{PyC}$ values and porosities of C/C–SiC composite vs. open porosities of C/C composites.

(see Fig. 4). Therefore, its intensity of (1 1 1) peak of Si phase is the highest. The $V_{PyC}$ value of CS-5 sample is higher than that of others samples (Table 1), which result in the highest (0 0 2) peak of C phase.

### 3.4. Flexural properties of C/C composite and C/C–SiC composite

The flexural strengths of the C/C composites and the C/C–SiC composites as a function of the open porosities of the C/C composites are illustrated in Fig. 6. According to the data in Table 1, Figs. 3 and 4, PyC volume ratio ($V_{PyC}$) of the C/C composite, Si volume ratio ($V_{Si}$) and porosity of the C/C–SiC composite are also plotted in Fig. 6 to analyze the factors affecting the flexural strength. It can be seen that the flexural strength of the C/C composite decreases from 127 MPa to 63 MPa while the $V_{PyC}$ also decreases when the porosity of the C/C composite increases. It indicates that the decrease of the flexural strength is caused by the decrease of the $V_{PyC}$ in the C/C composite.

Fig. 6 also shows that the flexural strength of the C/C–SiC composite is 38 MPa (CS-2) ~83 MPa (CS-4) higher than that of the C/C composite. This reveals that after RMI processing, SiC and unreacted Si improved the strength. The flexural strength of the C/C–SiC composite first increased slightly then decreased when the porosity of the C/C composite increased. It can be seen that CS-4 sample has the highest flexural strength (132 MPa) among the four types of composites. The mechanical properties of the C/C–SiC composites are not only influenced by the Si infiltration and Si/C reaction, but also affected by the content of PyC[23] and porosity[24] of the C/C–SiC composites. The PyC plays an important role in the load bearing during the bending tests. However, pore in the C/C–SiC composite is a weak phase which can reduce the flexural strength of the composite. CS-5

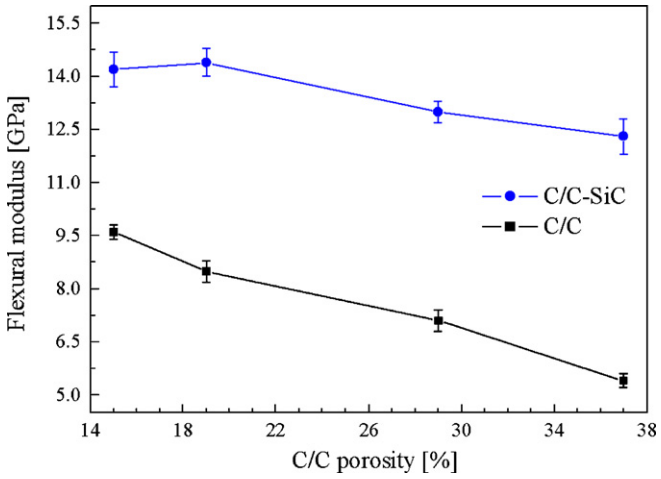


Fig. 7. Flexural moduli of C/C composites and C/C–SiC composites vs. open porosities of C/C composites.

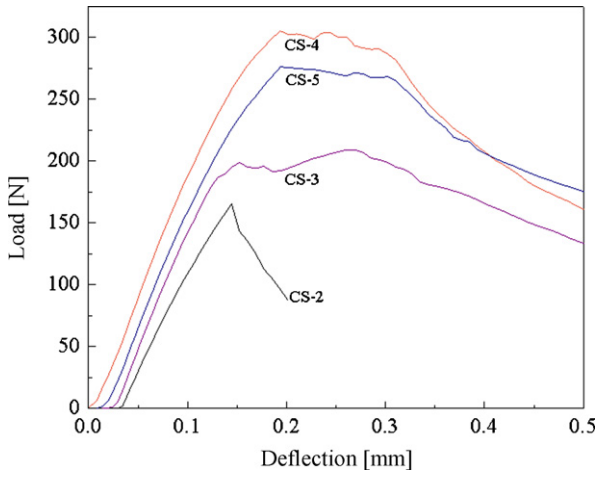


Fig. 8. Typical load–deflection curves of C/C–SiC composites.

has the highest $V_{PyC}$ among the four types of composites, which could lead to a higher mechanical property. However, it also has the highest porosity that decreased the flexural strength of CS-5 sample; that is the reason why its strength is little lower than that of CS-4 sample. Comparing the flexural strengths of the C/C–SiC composites with $V_{Si}$ values in Fig. 6, it can be seen that CS-2 sample has the highest $V_{Si}$ value and its flexural strength is the lowest among the four types of composites. This result indicates that higher $V_{Si}$ in the composite does not lead to a higher mechanical property of C/C–SiC composite.

The flexural moduli of the C/C composites and the C/C–SiC composites are plotted in Fig. 7. The modulus is decided by the modulus and volume ratio of the matrix and carbon fiber in the composites, as well as carbon fiber direction. Fig. 7 reveals that CS-4 sample processes the highest Young's modulus because it contains more PyC whose modulus is much higher than those of Si or SiC phases. The modulus of CS-5 sample is lower than that of CS-4 sample because its porosity is the highest among the four types of composites; the pores did not contribute to the modulus of the composite.

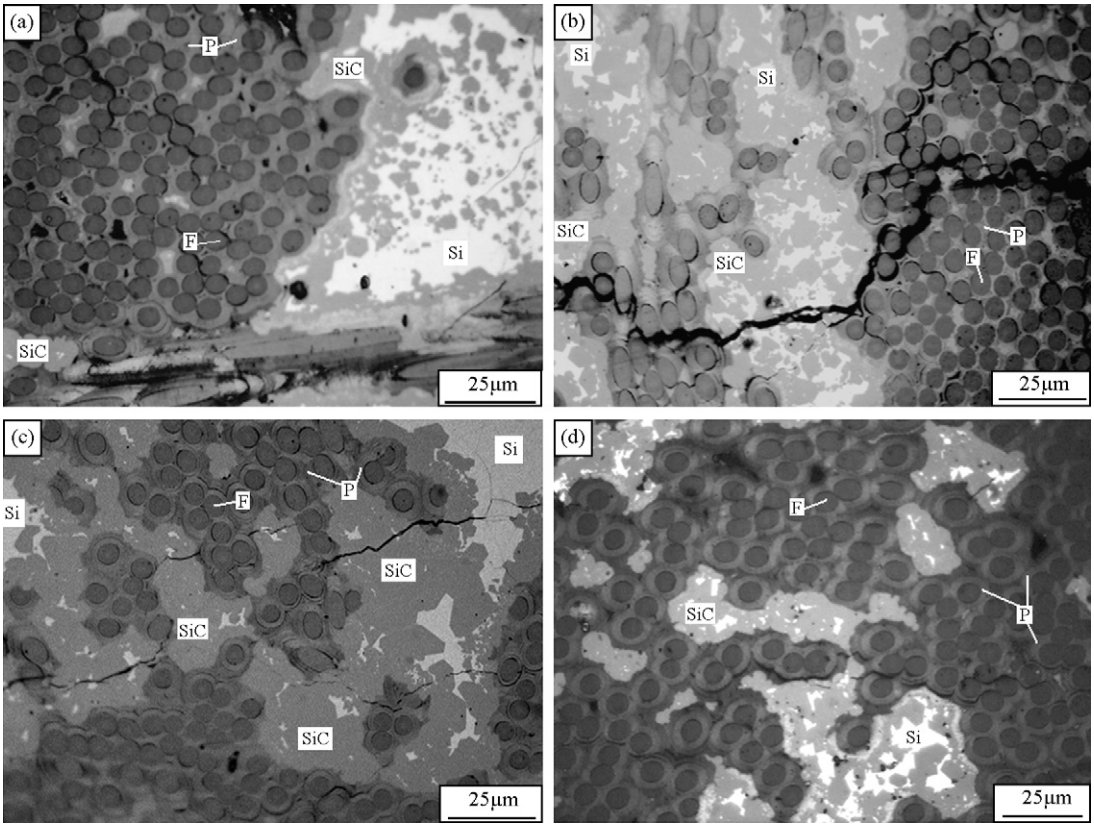


Fig. 9. Optical micrographs of polished surfaces of (a) CS-2, (b) CS-3, (c) CS-4, and (d) CS-5. F, carbon fiber; P, PyC.

Fig. 8 shows the typical load–deflection curves of the C/C–SiC composites, which can reveal the fracture behavior of the C/C–SiC composites. We can see that the load first increases linearly with the increase of the deflection. When the load closes to the maximum value, the changing trend of the load is different. The load of CS-2 sample decreases sharply which indicates a brittle failure behavior. CS-2 sample was infiltrated with the most Si (see Fig. 4) and Si is the brittle phase which contributes little to the toughness of CS-2 sample. In contrast, the curves of CS-3–CS-5 samples show that the loads decrease gradually. This is attributed to the increase of $V_{PyC}$ and the decrease of $V_{Si}$ in the composites. It can also be seen that the slope of the straight line in each curve is different, which reflects the flexural modulus of the composite. A higher strength modulus of the composite has a higher slope. CS-4 sample processes the highest slope, which is corresponding to results of Fig. 7.

The interfacial characteristics of fiber and matrix also affect the mechanical properties of C/C–SiC composite. It is necessary to analyze the microstructures of the C/C–SiC composite for further understanding of the relationship between the properties and the material processing.

### 3.5. Micrograph of C/C–SiC composite

The optical micrographs of the C/C–SiC composites are shown in Fig. 9(a)–(d). It reveals the distribution and different contents of carbon fiber, PyC, SiC and Si in the composites (each phase has been denoted in the figure). After the CVI processing, carbon fiber was surrounded by PyC ring. The thickness of PyC around interfiber is thinner than that of PyC around interbundle because the space in interfiber is much smaller than that in interbundle. This result was consistent with our previous research.[19] With the increase of CVI time, the PyC layer around interfiber becomes thicker. It can be seen that thickness of PyC layer in CS-5 sample (Fig. 9(d)) is much higher than that of PyC layer in CS-2 sample (Fig. 9(a)).

SiC layer was formed through the reaction between PyC and Si during the RMI processing, while carbon fiber was not damaged (see Fig. 9(a)–(d)). Therefore, the excellent mechanical property (especially tensile strength and modulus) of carbon fiber can be maintained. For the formed SiC layers, the interface between SiC and C phases appears continuous, while the interface between Si and SiC phases is rough. The different interfaces originated from the different reaction mechanisms between Si and C during RMI processing.[25]

Si still exists in the C/C–SiC composite (Fig. 9(a)–(d)) because it did not react with PyC completely. The different porosities and structures of the C/C composites lead to different free Si amount in the C/C–SiC composite. Fig. 9(a) shows that CS-2 sample has the most Si amount among the four types of composites. This phenomenon is coincident with the result of Si volume ratio (Fig. 4) and XRD analysis (Fig. 5). Si filled the pores in the C/C composite, and improved its mechanical property. However, Si was a brittle phase and mainly conglomerated in the large pores of the C/C composite, contributing little to the flexural strength of the C/C–SiC composite. It can also be seen from Fig. 9(a)–(d) that microcracks exist in the matrix and fiber–matrix debondings occurs in the composites. RMI processing was carried out at 1550 °C; then the composite was cooled down to room temperature. The thermal mismatch between matrix (PyC, SiC and Si phase) and reinforcement (carbon fiber) may cause the appearance of interfacial debonding and microcracks.[14,26]

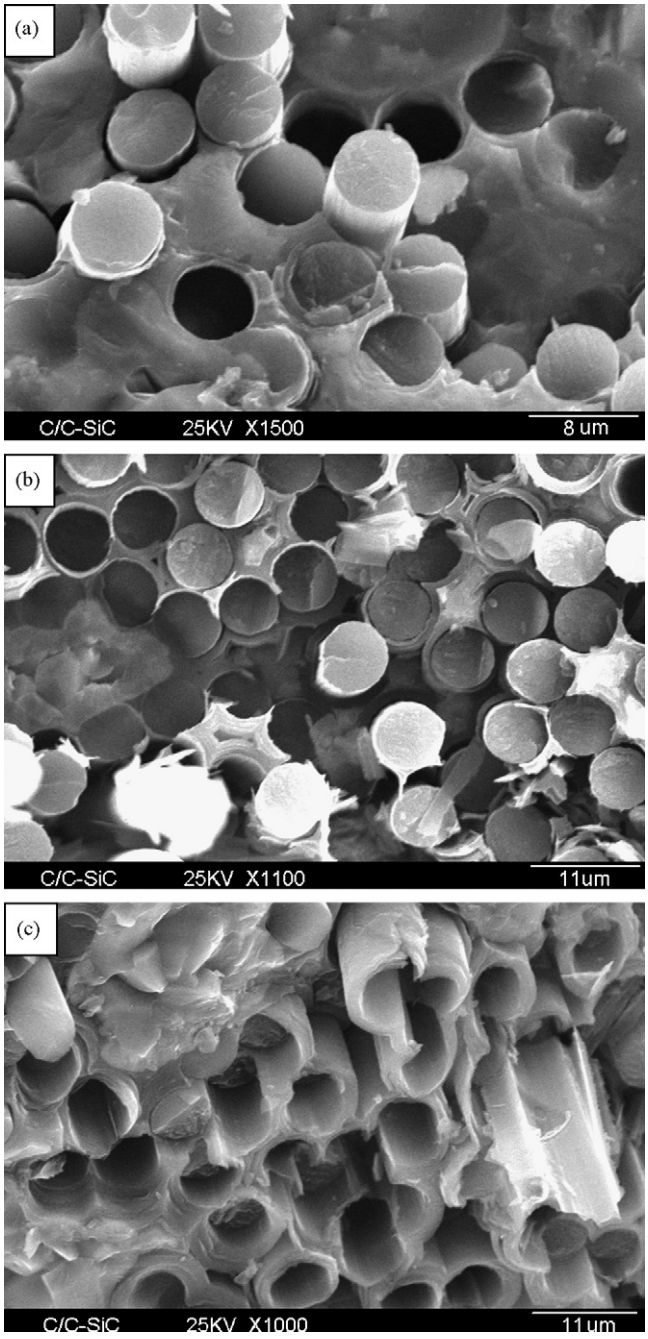


Fig. 10. SEM micrographs of fracture surface of (a) CS-2, (b) CS-4, and (c) CS-5.

The fracture surfaces of the C/C–SiC composites after three-point-bending tests are shown in Fig. 10. The micrograph of CS-2 sample (Fig. 10(a)) reveals that more residual Si is located in interspaces of the fiber bundles because the C/C composite was porous. In the fracture surface of CS-4 sample (Fig. 10(b)),

no fiber pull-out was observed. It indicates that the interface bonding between fiber and matrix is strong. The PyC layer around the fiber in CS-5 sample (Fig. 10(c)) is much thicker than that of the other composites. It can also be seen that many fibers pull-out and pores in the composites which will reduce the mechanical properties.

## 4. Conclusions

C/C–SiC composites were rapidly manufactured by a thermal gradient CVI method using kerosene as a precursor, combined with reactive melt infiltration method. The increasing porosity of C/C composite facilitates the infiltration of Si. The density of the C/C–SiC composite decreased from 2.31 g/cm$^3$ to 2.02 g/cm$^3$ and whose open porosity increased from 1.7% to 5.5% with the increase of porosity of the C/C composite. β-SiC, Si and C phases coexisted in the C/C–SiC composite after the RMI processing. The flexural strength and modulus of the C/C–SiC composite are much higher than those of the C/C composite. The C/C–SiC composite derived from the C/C composite with CVI time of 4 h (porosity of 19.7%) had the highest flexural strength (132MPa) and flexural modulus (about 14.4 GPa).

## Acknowledgements

This work was funded by National Natural Science Foundation of China (No. 50802073) and The Natural Science Foundation of Shaanxi Province (No. SJ08-ZT05). We also thank Dr. Daxiang Yang and Dr. Lixue Zhang for their help in revising this paper.

## References

1. Krenkel, W. and Berndt, F., C/C–SiC composites for space applications and advanced friction systems. *Mater. Sci. Eng. A*, 2005, **412**, 177–181.
2. El-Hija, H. A., Krenkel, W. and Hugel, S., Development of C/C–SiC brake pads for high-performance elevators. *Int. J. Appl. Ceram. Technol.*, 2005, **2**, 105–113.
3. Kermc, M., Kalin, M. and Vizintin, J., Development and use of an apparatus for tribological evaluation of ceramic-based brake materials. *Wear*, 2005, **259**, 1079–1087.
4. Stadler, Z., Krnel, K. and Kosmac, T., Friction behavior of sintered metallic brake pads on a C/C–SiC composite brake disc. *J. Eur. Ceram. Soc.*, 2007, **27**, 1411–1417.
5. Krenkel, W., Carbon fiber reinforced CMC for high performance structures. *Int. J. Appl. Ceram. Technol.*, 2004, **1**, 188–200.
6. Delhaes, P., Chemical vapor deposition and infiltration processes of carbon materials. *Carbon*, 2002, **40**, 641–657.
7. Golecki, I., Rapid vapor-phase densification of refractory composites. *Mater. Sci. Eng. R. Rep.*, 1997, **20**, 37–124.
8. Zhang, Y. N., Xu, Y. D. and Lou, J. J., Braking behavior of C/SiC composites prepared by chemical vapor infiltration. *Int. J. Appl. Ceram. Technol.*, 2005, **2**, 114–121.
9. Nie, J. J., Xu, Y. D. and Zhang, L. T., Microstructure and tensile behavior of multiply needled C/SiC composite fabricated by chemical vapor infiltration. *J. Mater. Proc. Technol.*, 2009, **209**, 572–576.
10. Odeshi, A. G., Mucha, H. and Wielage, B., Manufacture and characterisation of a low cost carbon fibre reinforced C/SiC dual matrix composite. *Carbon*, 2006, **44**, 1994–2001.
11. Zhong, J. H., Qiao, S. R. and Lu, G. F., Rapid fabrication of C/C/SiC composite by PIP of HMDS. *J. Mater. Proc. Technol.*, 2007, **190**, 358–362.
12. Fitzer, E. and Gadow, R., Fiber-reinforced silicon carbide. *Am. Ceram. Soc. Bull.*, 1986, **65**, 326–335.
13. Hillig, W. B., Making ceramic composites by melt infiltration. *Am. Ceram. Soc. Bull.*, 1994, **73**, 56–62.
14. Krenkel, W., Microstructure tailoring of C/C–SiC composites. *Ceram. Eng. Sci. Proc.*, 2003, **24**, 471–476.
15. Li, J. G. and Hausner, H., Reactive wetting in the liquid-silicon/solid-carbon system. *J. Am. Ceram. Soc.*, 1996, **79**, 800–873.
16. Gern, F. H. and Kochendörfer, R., Liquid silicon infiltration: description of infiltration dynamics and silicon carbide formation. *Compos. A*, 1997, **28**, 355–364.
17. Yang, J. and Ilegbusi, O. J., Kinetics of silicon–metal infiltration into porous carbon. *Compos. A*, 2000, **31**, 617–625.
18. Favre, A., Fuzellier, H. and Suptil, J., An original way to investigate the siliconizing of carbon materials. *J. Ceram. Int.*, 2003, **29**, 235–243.
19. Wang, J. P., Qian, J. M., Jin, Z. H. and Qiao, G. J., Microstructure of C/C composites prepared by chemical vapor infiltration method with vaporized kerosene as a precursor. *Mater. Sci. Eng. A*, 2006, **419**, 162–167.
20. Wang, J. P., Qian, J. M., Qiao, G. J. and Jin, Z. H., A rapid fabrication of C/C composites by a thermal gradient chemical vapor infiltration method with vaporized kerosene as a precursor. *Mater. Chem. Phys.*, 2007, **101**, 7–11.
21. Wang, J. P., Jin, Z. H. and Qiao, G. J., Rapid fabrication of C/C–SiC composites. *Key Eng. Mater.*, 2006, **317–318**, 159–165.
22. Wang, J. P., Jin, Z. H., Qian, J. M. and Qiao, G. J., Study of rapid fabrication and microstructure of C/C–SiC composites. *Rare Met. Mater. Eng.*, 2006, **35**, 223–226.
23. Zhu, Y. Z., Huang, Z. R., Dong, S. M. and Yuan, M., Correlation of PyC/SiC interphase to the mechanical properties of 3D HTA C/SiC composites fabricated by polymer infiltration and pyrolysis. *New Carbon Mater.*, 2007, **22**(4), 327–331.
24. Reynaud, C., Thévenot, F., Chartier, T. and Besson, J. L., Mechanical properties and mechanical behaviour of SiC dense-porous laminates. *J. Eur. Ceram. Soc.*, 2005, **25**(5), 589–597.
25. Schulte-Fischedick, J., Zern, A. and Mayer, J., The morphology of silicon carbide in C/C–SiC composites. *Mater. Sci. Eng. A*, 2002, **332**, 146–152.
26. Kumar, S., Kumar, A. and Shukla, A., Thermal-diffusivity measurement of 3D-stitched C–SiC composites. *J. Eur. Ceram. Soc.*, 2009, **29**(3), 489–495.